

Entanglement reduction induced by geometrical confinement in polymer thin films

Nicolás A. García^{*,†} and Jean-Louis Barrat^{†,‡}

[†]*Institut Laue-Langevin, 71 Avenue des Martyrs, 38042 Grenoble, France*

[‡]*Univ. Grenoble Alpes, CNRS, LIPHY, 140 Rue de la Physique, 38402 Saint-Martin-d'Hères, France*

E-mail: garciana@ill.fr

Abstract

We report simulation results on melts of entangled linear polymers confined in a free-standing thin film. We study how the geometric constraints imposed by the confinement alter the entanglement state of the system compared to the equivalent bulk system using various observables. We find that the confinement compresses the chain conformation uniaxially, decreasing the volume pervaded by the chain, which in turn reduces the number of the accessible inter-chain contact that could lead to entanglements. This local and non-uniform effect depends on the position of the chain within the film. We also test a recently presented theory that predicts how the number of entanglements decreases with geometrical confinement.

Introduction

Viscoelastic properties of polymer in melts or concentrated solutions depend strongly on the molecular weight of the polymer chains. The main effect of increasing molecular weight is

the apparition of topological constraints between the chains called entanglements. These constraints are a universal aspect of polymer physics and arise in any flexible polymer if the chain is sufficiently long and the concentration is high enough. Under these conditions, the effect of entanglements becomes so relevant that system dramatically changes their physical properties such as viscosity, diffusion, rheological and mechanical behavior.

Nowadays, the most extended and successful theory regarding entangled polymer dynamics is the *Tube model* presented by Doi and Edwards¹ and extended as *Reptation model* by de Gennes^{2,3} which provided a framework for understanding many aspects of the underlying polymer physics in both regimes: melt and solution. The theory averages the collective effect of all surrounding chains over a given strand to a tubelike-region of confinement whose central axis is one segment of the called *primitive path (PP)*. In this approach, the primitive path is an essential theoretical concept introduced by Edwards^{4,5} and defined as the shortest path connecting the two ends of the chain preserving its topology. As a result of this confinement in a virtual tube, the strand moves back and forth performing a *slithering motion* inside the tube (reptates). Despite its conceptual simplicity this theory proved to be a powerful tool to understand polymer dynamics and their quantitative predictions fit quite well with experimental results.

Polymer thin films have numerous applications (e.g., coatings, dielectrics, adhesives, lubricants⁶⁻⁸), but are also of fundamental interest. Thin films below a certain thickness induce geometrical confinement so that the polymeric material exhibits unusual physical properties compared to its bulk behavior.^{9,10} Viscoelastic properties are not the exception and are affected below of a certain confinement strength. This is clearly reported in experiments;^{11,12} however, the precise link between these modifications and the changes in the topological structure, or entanglement network, are not fully understood yet. Indeed, the manner in which the entanglement network is modified under confinement is a subject of current interest.

As entanglements are not directly observable via experiments, numerical simulations

are an essential tool to study their nature. Since entangled chains have very long relaxation times, classical Molecular Dynamics is quite limited for such studies. Recently new coarse-graining techniques were introduced to simulate entanglements such as *slip-springs* or *slip-links* which introduce a temporary attractive force between nearby beads, imitating entanglement effects.¹³⁻¹⁸ However, in such studies, the effect of heterogeneity or confinement on the slip link (entanglement) density has to be specified somewhat arbitrarily, so that it becomes essential to inform such techniques using a more microscopic approach, numerical or theoretical.

Recently, a step in this direction was performed by extending the principle of conformational transfer of Silberberg to predict the entanglement reduction in thin films or cylinders as a function of the aspect ratio between the film thickness (or cylinder radius) and the end-to-end chain distance.^{19,20} The predictions of the theory were tested using molecular dynamics simulations, however in weakly entangled systems.

In this paper, we extend this analysis to more strongly entangled systems, using a technique that uses ultrasoft potentials to speed up the simulation.²¹ Our primary aim is to unveil how, in a thin film built with linear polymers, the geometrical confinement acts as an external field that modifies the entanglement state of the system, and what are its most relevant consequences. The article is organized as follow: In the next section, we describe the simulation model and the methods and protocols used in our study. Then, the section “*Results and discussion*” presents the results, with five subsections addressing different aspects of the confinement effect. The main conclusions are summarized in the last section.

Model and methods

The model is based on a new original approach to simulate entangled of polymer in melt or concentrated solution condition, reported in an earlier work,²¹ and which was recently successfully used to study polymer brushes under shear flow.²²

The main idea is to use a pseudo-continuous model of a polymer solution, consisting of long chains interacting through a soft potential field. The motion is then resolved using Brownian dynamics with large time steps.

The motion of C chains in dense conditions, each described by a continuous curve $\mathbf{R}_c(t, s)$, with variables t for time and $s \in (0, 1)$ as the monomer index, is solved numerically. The continuous backbone s , uses a finite number of discrete points $j = 1, 2, \dots, J$ to, generally, oversample the chains. Choosing $J = N$ the chain is reduced to the standard bead-spring model, which for this soft-potential has gaps that may allow chains to cross each other. This is a novelty aspect on this coarse-graining, where the crosses are avoided oversampling enough the chains to suppress the gaps along the backbone effectively. In this work, we found that $J = 4N$ is sufficient to describe the chains in all our simulations well.

Every chain has N degrees of freedom that correspond to the usual Rouse modes (or alternatively to N beads through the usual Rouse transformation, see Ref. 21), and follows the stochastic first order equation of motion:

$$\zeta \frac{\partial \mathbf{R}_c(t, s)}{\partial t} = F_s - N \nabla V_c + \sqrt{2k_B T \zeta} \mathbf{W}_c(t, s) \quad (1)$$

here $\zeta = N\zeta_0$ is the friction coefficient of the chain center of mass.

The strength of the thermal noise is modeled by a Wiener process $\langle \mathbf{W}_c(t, s) \mathbf{W}_{c'}(t', s') \rangle = \delta_{cc'} \delta(t - t') \delta(s - s')$.

In Eq. 1 F_s models the bonded interaction (bead-spring):

$$F_s = \left(\frac{3k_b T}{Nb^2} \right) \frac{\partial^2 \mathbf{R}_c(t, s)}{\partial s^2}. \quad (2)$$

where Nb^2 is the mean square end-to-end distance of a free chain, and can be combined with other parameters to define the microscopic unit of time, $\tau = \zeta_0 b^2 / k_B T$.

V_c describes the nonbonded interactions between chains:

$$V_c = \sum_{c'=1}^C \int_0^1 \Phi[\mathbf{R}_c(t, s) - \mathbf{R}_{c'}(t, s')] ds' \quad (3)$$

Here, we propose as $\Phi(r)$ a soft potential model through a combination of Gaussian functions, that takes into account both relevance interaction; excluded volume and attractive force:

$$\Phi(r) = \left(\frac{N}{J}\right) k_B T \left[(w + 1) e^{-r^2/2\lambda^2} - w e^{-r^2/4\lambda^2} \right] \quad (4)$$

where $w \geq 0$ is a parameter to control the relative weight of the attractive part. At this point, it is important to remark that in potentials such as the one proposed in Eq. 4 a problem of thermodynamic stability may arise, so the selection of the value for w is not a trivial question. In fact is well known²³⁻²⁵ that when interacting bodies without an infinitely repulsive core (i.e., finite force value at zero separation) also interact through attractive forces, if the attraction is too strong the weak short-range repulsion may not be sufficient to prevent a “collapse” of the system allowing all particles eventually to overlap in a finite region of space: the thermodynamic catastrophe occurs. Well-defined criteria to ensure thermodynamic stability were derived by Fisher and Ruelle.^{26,27} In this work, we determined a thermodynamic safety interval of values for w applying these criteria following a straightforward approach proposed in Ref. 28. We found that the stability condition is $w \geq (2^{3/2} - 1)^{-1}$ for this parameter, and we use the value $w = 0.5$ for all the simulation reported here. More details are given in Appendix I.

A central point of this coarse-grained description is the use of an approximate but high-speed method of evaluating the interparticle forces. The technique involves splitting the force into two terms and evaluate them on a staggered grid. The first term takes into account short-range interactions and the second one the long-range contributions. The short-range part is calculated through linearization of the gaussian force, and the long-range part using a convolution between the density field and the potential in Fourier space, where the periodic

boundary conditions are incorporated naturally.

The matrix-matched nature of this problem allows the implementation of a transparent parallelization into the GPU paradigm, which enabled us to take advantage of these high-performance devices. Hence, the simulation code was programmed in CUDA with an optimized implementation of the available memories and all simulations reported in this manuscript were run in two GPU cards Nvidia Quadro P1000 both included in a conventional desktop computer.

In order to reach the equilibrium state quickly, we use the method proposed in Ref. 29. The method starts by locating randomly C monomer in a box with the proper dimensions to set the target density. Initially, there are C *chains* with one monomer each one. Then, the method adds monomer systematically along the chain backbone, rescaling the box properly to conserve the density. This process is repeated until the desired chain-length is reached. We then run a simulation in which the mean square displacement (MSD) of the central monomer is followed and ensure that the chains diffuse enough distance to sample the film thickness adequately and the equilibration time is already passed before starting to compute observables.

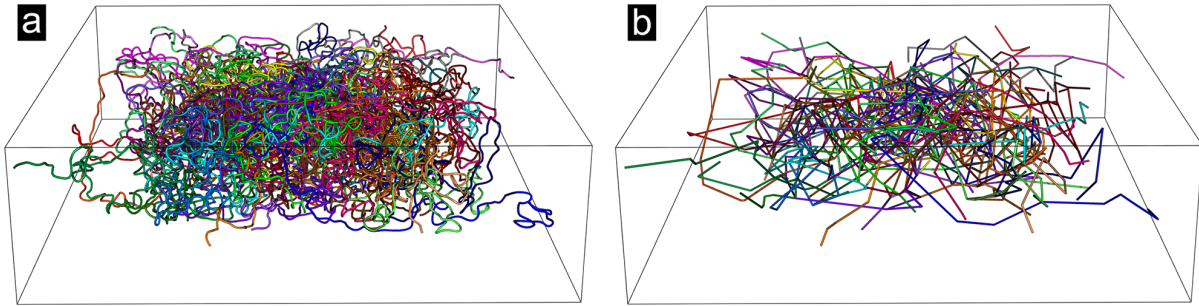


Figure 1: (a) A free-standing film of thickness $h_{eff} \sim 28$ containing $C = 64$ chains of length $N = 512$ built with this model. The 3D box container is not the simulation box and is just shown to improve visualization. The entire chains are shown, without taking into account the periodic boundary conditions. (b) Primitive Path chain reduction obtained by $Z1$ algorithm. The label color is preserved between original chains and the corresponding primitive paths.

The dimensions of the cubic simulation box were chosen to create a system with initial monomer density of $\rho_i = 0.12$, so $L_{box}^3 = NC/\rho_i$. As a result of the attractive interaction, the

system spontaneously forms a thin film in a central region of the box, reaching an equilibrium density of $\rho_f = 0.277$ inside the film. This value is determined from the density profile shown in Figure 2. This final density depends on the parameter w which, as we mentioned before, is fixed to $w = 0.5$ in our study. We also confirmed that the largest radius of gyration is roughly three times smaller than L_{box} , which should be enough to ensure that the chains do not interact with their periodic images. Figure 1a shows an instantaneous configuration of a free-standing film obtained with this preparation protocol.

We have chosen to work with monodisperse linear chains of $N = 512, 1024$ and 2048 monomers conforming self-confined films containing $C = 8, 16, 32, 64, 128, 256,$ and 512 chains. Also, in order to have systems of reference for the different chains lengths, it was performed simulations of $C = 64$ chains with $N = 512, 1024$ and 2048 monomers with the same parameters as before but in bulk conditions, i.e., setting the box dimension correctly to get a constant density of $\rho_{bulk} = 0.277$.

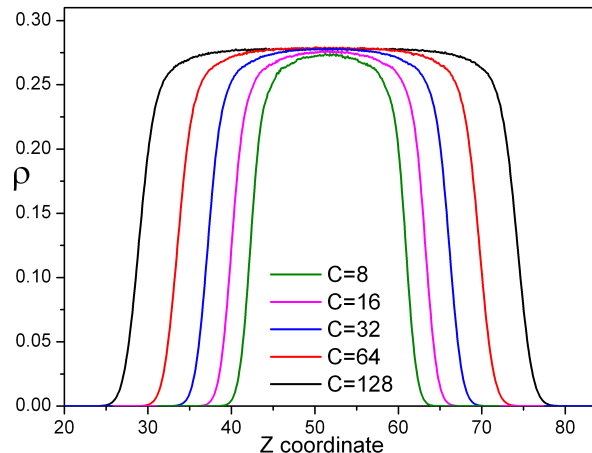


Figure 2: Monomer density profiles for a chain length $N = 1024$ and films built with $C = 8, 16, 32, 64$ and 128 chains.

Figure 2 shows the monomer density profiles for some films built with chains of length $N = 1024$. The film thickness is obtained by fitting these profiles with the following hyperbolic tangent function as a function of the z coordinate:

$$\rho(z) = \frac{\rho_0}{2} \left(1 - \tanh \left(\frac{|z - z_0| - \xi}{d} \right) \right) \quad (5)$$

where ρ_0 is the density in the interior of the film, ξ is the half width of the interior thickness, z_0 is the position of the middle film, and d is a measure of the width of the interface, which is a consequence of the density fluctuations near the surface. Finally, the effective film thickness can be reduced to $h_{eff} = 2\xi$. By this measure, the thickness of the profiles in Figure 2 were $\sim 17.6, 22.2, 28.0, 35.3,$ and 44.4 in units of the monomer diameter λ and the inner density for all of them is $\rho = 0.277$. As is expected, these values are in good agreement with the direct estimation of the thickness from $h_{eff} = (\rho_i/\rho_f)L_{box}$.

To characterize the behavior of some important vectors (segments of PP , \mathbf{R}_{ee} , etc.), we will use the second Legendre polynomial:

$$P_2 = \frac{3}{2}\langle \cos^2(\theta) \rangle - \frac{1}{2} \quad (6)$$

where θ is the angle between the vector under study and a given *fixed* direction of interest defined by a unit vector called the director, which will be explicitly indicated in each case. P_2 is widely used to study nematic order in diverse systems (liquid crystal, etc.), and is also helpful to quantify the behavior of a vector (or a vector field) around a given direction of interest. This order parameter lies within the interval $-0.5 \leq P_2 \leq 1$, where a value of $P_2 = 1$ indicates that vectors under analysis align perfectly with the direction of reference, $P_2 = 0$ corresponds to an isotropic distribution around the reference direction. The negative value of the lower bound, -0.5 , corresponds to vectors all oriented in a plane perpendicular to the director.

The topological analysis of the systems presented in the following are all performed using the *Z1 algorithm*,³⁰⁻³³ a method based on the MD trajectories which finds entanglement by geometrical minimization. In this code, all chain ends are maintained them fixed in the space, excluded volume interactions are disabled, but the chain uncrossability condition is preserved. Then, a set of geometric operations are applied over of all this *pseudo*-chains, which monotonically reduce its contour lengths. Eventually, the method builds a PP for each

chain thereby reducing the linear polymer system to an entanglement network of *PPs*. This iterative geometrical minimization procedure terminates as soon as the mean length of all *PPs* has converged. Figure 1b shows the *PP* network obtained by applying *Z1* algorithm to the film plotted in Figure 1a, here is important to remark that the chains are drawn entirely, i.e., without cutting at the periodic boundary conditions of the simulation box. As a result, some chains (or extremes) which appear isolated, have entanglements, as they cross the box boundary and are effectively surrounded by periodic images of the chains represented.

Additionally, the *Z1* code provides the statistical properties of the underlying topological network but also the positions of the interior *kinks*^{31,32} along the three-dimensional *PP* for each chain. For long chains, the number of kinks is proportional to the number of entanglements and in this context, both terms can be considered as *equivalents*. In this approach, self-entanglements (intramolecular knots) are neglected, as they represent a small fraction and are irrelevant for most polymeric systems.

Results and discussion

Statistics of entanglements in bulk

As a reference, we start by using the *Z1* algorithm³⁰⁻³³ to perform a topological analysis of the bulk system configurations.

Figure 3a shows the temporal evolution of the total numbers of entanglements per chain (Z) after equilibration. This number fluctuates slightly around its average value, which is an indicator that the systems were well equilibrated. Moreover, as is expected in bulk at fixed density, the average value $\langle Z \rangle$ of the number of entanglements per chain increases linearly with the chain-length N , with a slope of $\alpha = 0.03125$ (Figure 3b). This slope is just the reciprocal of the entanglement length $N_e = 1/\alpha = 32$ (in number of monomers), which can be used to characterize the crossover between the Rouse and Reptation regimes. In the reptation model, N_e is defined as the arc length of a chain with mean-square end-to-end

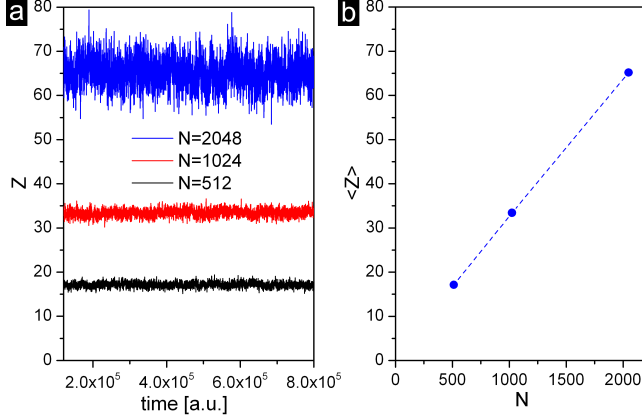


Figure 3: (a) Temporal evolution of the average number of entanglements per chain (Z) measured by the $Z1$ algorithm after equilibration for three different melts built with $C = 64$ chains of lengths $N = 512, 1024$ and 2048 in bulk conditions at $\rho_{bulk} = 0.277$. (b) Temporal average number of entanglements per chain $\langle Z \rangle$ as a function of the chain-length N .

distance equal to tube diameter a ($N_e = (a/b)^2$, b being the statistical segment length).

The statistic of entanglements in bulk systems is well explained by the *chain packing model*.^{34–36} Mostly, the idea is that the larger the dimensions of a chain, the greater the volume pervaded by that chain, so the greater the number of other neighbors chains it will encounter and with which it might entangle. In this model, N_e is defined as the ratio of the pervaded volume V_p to the real volume occupied by the chain V_c . Although V_p is not easy to calculate, a well-accepted estimate is proportional to the volume covered by one of their characteristic lengths of the chain: R_{ee} or R_g . Thus, the pervaded volume can be estimated as $V_p \propto R_{ee}^3$ while the effective volume occupied by the chain is $V_c \propto N\lambda^3$. This model assumes that an entanglement arises when the molecular weight and the concentration are such that at least two chains share the same pervaded volume, i.e., $V_p/V_c \sim 2$.

These volumes scale differently with molecular weight, $V_p \propto N^{3/2}$ while $V_c \propto N$. As a result, increasing the chain length increases the number of chains that are allowed to share the same pervaded volume, favoring the interchain contacts that lead to entanglements. In the following, we will, however, see that this model is not sufficient to explain the statistics of entanglements in confined systems.

Global impact of the confinement on the entanglements

Figure 4 shows the total number of entanglements per chain compared to its bulk value, $\langle Z \rangle / \langle Z \rangle_{bulk}$, for thin films of various thickness. The film thickness h_{eff} is normalized here using the average end-to-end distance in bulk conditions for the same chain length. This normalization is guided by the proposal of reference,¹⁹ which suggests that the corresponding curve should be universal in the limit of large molecular weight.

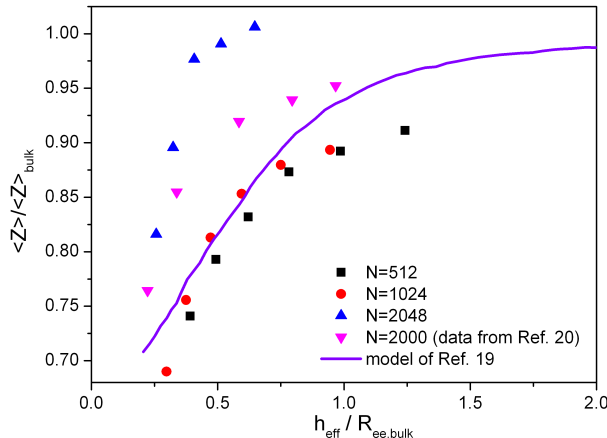


Figure 4: Normalized reduction of entanglements per chain as a function of confinement for all free-standing films thicknesses studied here, for chain lengths $N = 512, 1024$ and 2048 . Data of a similar system reported in Ref. 20 and the model proposed in Ref. 19 are also included.

Globally, we find that confinement leads to a decrease in the average number of entanglements per chain. Qualitatively, this result is in good agreement with the one observed in experiments,^{10,37,38} simulations,^{17,39,40} and with the theoretical model proposed in Ref. 19. However, Figure 4 shows that, quantitatively, there is a notable difference between our results and the model proposed by Sussman and coworkers.¹⁹ Figure 4 clearly shows that the model accounts reasonably well for the data obtained for shorter chains, but strong deviations are observable for thin films made of long chains. In those films, the decrease of the entanglements is observed only for films that are significantly thinner than the size of the unperturbed chain. Data for $N = 2000$ extracted from a recent manuscript²⁰ displays a similar trend. In the next section, we discuss possible reasons for the origin of the discrepancy

between theory and simulation.

The Z1 algorithm also provides the primitive path (*PP*) conformation of each chain, from which it was possible to determinate the position of entanglements within the film. A spatially resolved profile of the entanglement density across the film is shown in Figure 5 and compared with the monomer density profile for films of different thickness built with chains of $N = 1024$ monomers.

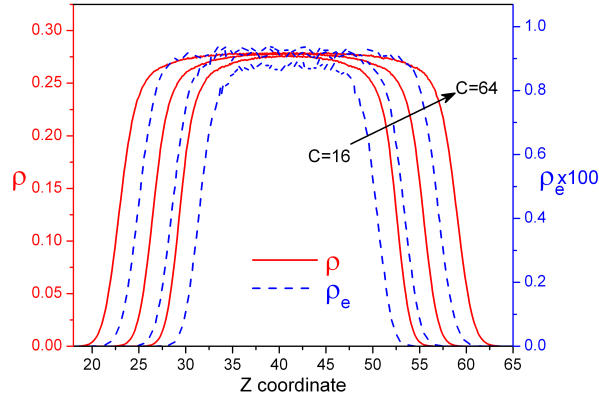


Figure 5: Monomer and entanglement density profiles. For $N = 1024$ and three films of $C = 16, 32$ and 64 chains respectively. Two different scales (left blue and right red axis) are used to plot these quantities in the same figure for comparison.

Is interesting to note in Figure 5, that entanglements sample the space uniformly within the film exhibiting a notable decrease only near to the surface.

Understanding the discrepancy between simulations and theory

The theoretical model presented in Ref. 19 is based on three fundamental hypothesis: (I) validity the principle of conformational transfer proposed by Silberberg,⁴¹ generalized to a thin film geometry, (II) the distribution of orientations of the end-to-end vector is made anisotropic by the geometric confinement, and this orientation distribution is directly communicated to the primitive path network, (III) the distribution of orientations at the *PP* scale is used to predict the changes in the entanglement network. In the following, we will analyze the validity of these assumptions for our simulations, in order to understand the origin of the observed discrepancy.

Hypothesis (I), involves a modification of the Silberberg model⁴¹ which treats the chain as a random walk using reflecting boundary conditions to compute changes to the chain conformation in the presence of a wall. The original model formulated by Silberberg consider the perturbation of chains near to one wall in space and makes quantitative predictions for the statistics of the chain conformations in the direction normal to the surface.

Following the philosophy of Silberberg, the authors of Ref. 19 proposed an extension of this idea for thin films. Two walls with reflecting boundary condition delimit the film, and the contribution of both surfaces are added to obtain the chain conformation inside the film. At first order, the early two reflections are taken into account. Formally, in analogy with the method of images in electrostatics, second and higher order reflections should also be taken into account, so that the final results involves summing an infinite series. Fortunately, due to the fast decaying of the superior order contributions, the convergence of the series is quick, and only a few terms are needed to reach an accuracy. This extended model allows one to predict the change in the normal component of the mean end-to-end vector as a function of the distance from the final random walk step to the surface, $R_{ee,z}^2(z)$. Integrating this function through the film thickness, it is possible to compute the global change in the normal component as a function of the film thickness. For further information on this approach see Ref. 19.

In Figure 6, the prediction of this extended Silberberg model for the perpendicular component of the bulk normalized mean end-to-end vector as a function of the normalized films thicknesses is compared with our simulation results for different chain length exhibiting an excellent agreement and supporting the validity of this first hypothesis.

Figure 6 also displays the normalized parallel components (R_{ee}^x, R_{ee}^y) averaged over the film thickness. As expected, these components are only slightly affected by confinement and exhibit a bulk-like behavior.

In order to check the second hypothesis (II), we analyzed the orientational probability distributions of the PP segments and R_{ee} vectors concerning the z -direction for different

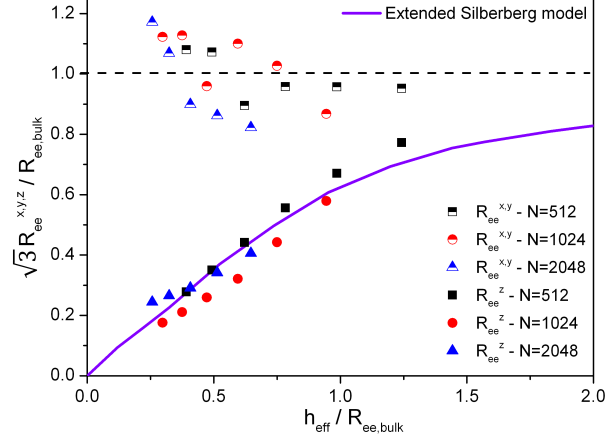


Figure 6: Root-mean-square components of the end-to-end as a function of the normalized film thickness for all thin films and chain lengths studied here. Filled symbols are the component normal to the surface of confinement R_{ee}^z for different chain-lengths, and the semi-filled symbols are the components parallel to the surface, $R_{ee}^{x,y}$. The continuous line is the prediction of the extended Silberberg model and the dashed black line is the bulk value $R_{ee,bulk}/\sqrt{3}$.

degrees of confinement, here expressed as $\delta = h_{eff}/R_{ee}$. These results are shown in Figure 7a, b and c where is immediately evident, at least globally speaking, the orientations present R_{ee} are not communicated to the PP length scale, shedding doubt on the validity of this second hypothesis. The chains are much more strongly oriented at the scale of the end-to-end vector than at the scale of the primitive path segments. The data in Figure 7a shows that as the confinement increases (δ decreases) the two distribution become peaked around zero, i.e., the chain tend to lie parallel to the interface. However, the order of magnitude of the effect is much more pronounced for the end-to-end vector than for the primitive path segments.

Furthermore, this difference becomes more notable for longer chains. The distributions for R_{ee} becomes more peaked for $N = 1024$ (Figure 7b) and even more for $N = 2048$ (Figure 7c) for a similar degree of confinement, while the orientation of the primitive path seems insensitive to the chain length and only slightly dependent on δ .

In addition to this global analysis, we have studied the local behavior of both vectors to assess the possible existence of a local correlation. We have evaluated a profile of the P_2

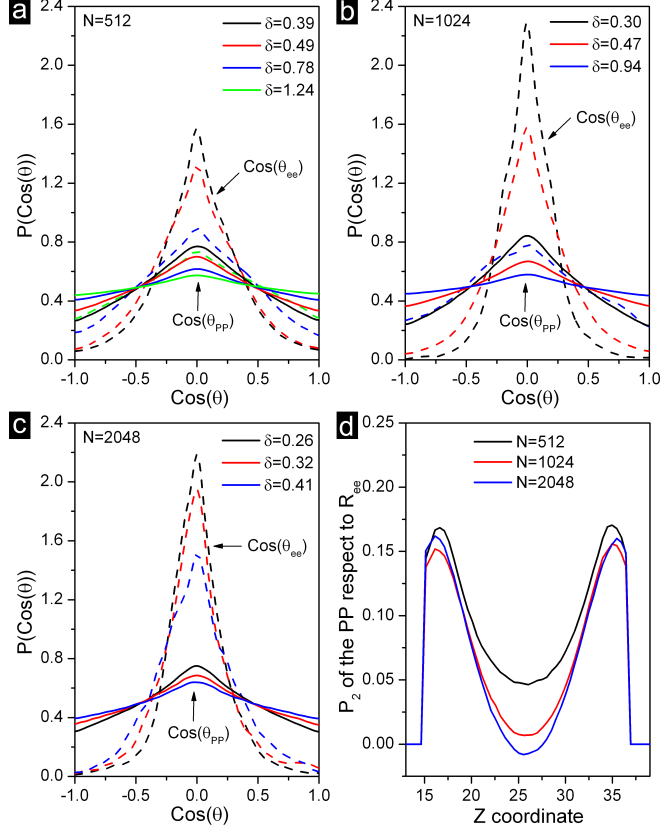


Figure 7: (a), (b), (c) Average distribution of the angle with respect to the z -axis of the PP segments (solid lines) and the R_{ee} vectors (dashed lines) for different chain lengths and confinement strength δ . (d) profile of the P_2 parameter evaluated using the angle defined between the PP segments and the R_{ee} vector.

order parameter for the angle between the end-to-end vector of a chain and the PP vectors (segments) belonging to this chain. The sketch in Figure 8 illustrates this idea and Figure 7d reports this observable.

The local correlation becomes more important near the surface, however, all values remain below $P_2 = 0.3$, indicating a very poor orientational correlation between these vectors. Moreover, the range over which the correlation is felt appears to be independent of chain length, and for longer chains, the correlation is completely lost in the middle of the film.

Clearly, these observations indicate that, while the extension of the Silberberg model gives an accurate picture of the global chain conformation, the primitive path is much less affected by confinement than expected in the theory. Indeed, the thickness over which the

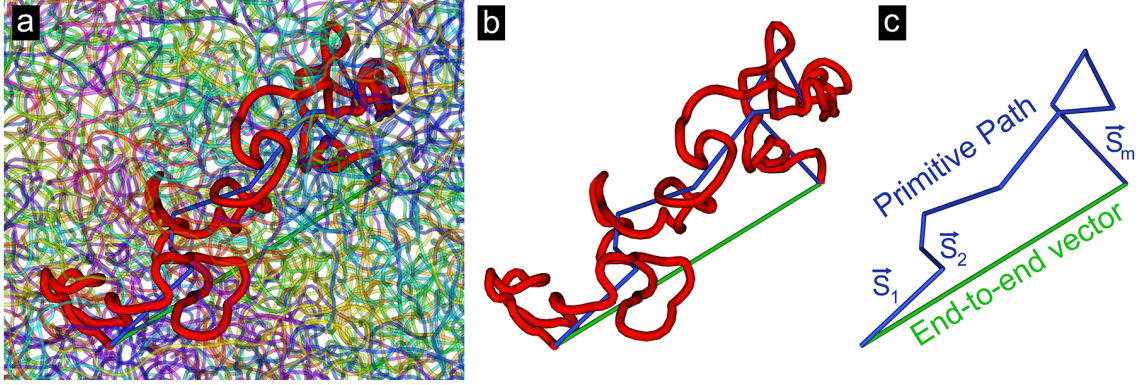


Figure 8: The method implemented to study the local orientational correlation between the PP segments and the end-to-end vector through P_2 . In all those images are shown the PP (in blue) and the end-to-end vector (in green). (a) Highlighted in red, a chain embedded in the film. All the others chains are thinned and transparent. In (b) all others chains were removed to improve visualization. (c) The segments S_1, S_2, \dots, S_m forming the PP are used to evaluate P_2 relative to the end-to-end vector.

orientation of the primitive path is affected does not appear to scale with molecular weight but is restricted to a finite thickness layer at the surface of the film. This leads to the deviation of $\langle Z \rangle / \langle Z \rangle_{\text{bulk}}$ from the h_{eff} / R_{ee} scaling reported in figure 4.

Chains conformations and the importance of surface effect

Heretofore, we have studied how the confinement affects the statistics of entanglements and the distributions of end-to-end vectors or primitive paths segment self-confined free-standing films. In this section, we investigate how the confinement alters the global shape of the chains.

The first set of descriptors are the three diagonal components of the inertia tensor (or gyration tensor) G_{xx} , G_{yy} and G_{zz} . The squared gyration radius can be expressed as $R_g^2 = G_{xx} + G_{yy} + G_{zz}$. Figure 9 shows the averaged value of these components normalized with the corresponding bulk value as a function of the position of the center of mass of the chain. To avoid redundancy of data, we report these observables for only two different thicknesses ($h_{\text{eff}} = 22.16$ blue lines, $h_{\text{eff}} = 44.32$ red lines) built with chains of $N = 512$ monomers, but the data obtained with varying lengths of chain are very similar.

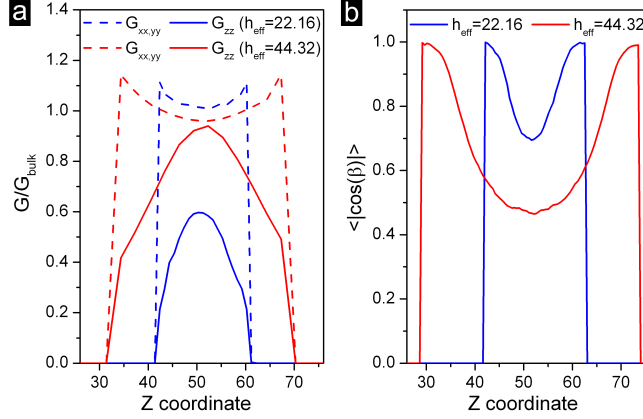


Figure 9: Profiles evaluated using the location of the center of mass of the chains within the film of (a) Bulk normalized and temporal-averaged components of the radii of gyration $G_{xx,yy}$ and G_{zz} , (b) Average-absolute value of the cosine director of the eigenvector associated with the minimum eigenvalue of the gyration tensor with respect to the surface of confinement. These observables were evaluated for two film thicknesses $h_{\text{eff}} = 22.16$ (in blue) and $h_{\text{eff}} = 44.32$ (in red).

In Figure 9a is possible to see that for both thicknesses (continuous lines) the component G_{zz} , associated with the direction of confinement, tends to induce a noticeable shrinking of the chains on that direction, i.e., the chains break their spatial isotropy and tend to adopt a flat shape near the surface. In counterpart, the components $G_{xx,yy}$ slightly change their values, increasing as much a 10% compared to their bulk value (dashed lines in Figure 9a), which is in good agreement with previous works.⁴²

Until now, we have used the tensor as is, expressed in the canonical system of reference $\{x, y, z\}$, i.e., without diagonalizing in its principal axes. By diagonalizing the G tensor and studying the cosine director of the eigenvector associated with the minimum eigenvalue (which represent the most important direction to where the chain is elongated), it is possible to know the main direction of this flatness. In Figure 9b is reported how the average orientation of this vector is dictated by the position of the chain within the film. Independently of the molecular weight, all chains are flat at the edges of the film, then this effect decreases monotonically while entering in the film. This idea is also in good agreement with the predicted compression of the end-to-end vector discussed in the previous section.

In Figure 9a and Figure 9b it is seen that the flattening alters the chain shape all across

the film thickness for this chain-length ($N = 512$, $R_g \sim 19.1$). In Figure 9a, at the edge of the thicker film ($h_{eff} = 44.32$, red lines) the chain compression reaches a maximum of around 60% compared to its bulk value as is evidenced in the component of the radius gyration perpendicular to the plane of confinement (G_{zz}). Then, the compression decreases monotonically along the film achieving a bulk-like state in the center. Considering here that the film thickness is around two times R_g (i.e., the chain size is comparable with the film thickness) it is reasonable that the chain whose center of mass is located roughly in the middle film adopt bulk-like conformations.

In the case of the thinner film ($h_{eff} = 22.16$, blue lines) the chains experience a stronger shrinkage at the boundary, and although the effect decreases inside the film, the bulk state is not reached in the center. Which is also reasonable due to this thickness is almost the half of the chain size ($2R_g$), so the chain conformation is strongly confined. Even in the center of the film the chain reaches only around half of its bulk size in the z -direction. This simple analysis provide an accurate picture of the chain conformations across the film.

Primitive path network under confinement

In this section, we study how the confinement impacts the primitive path network. To quantify this confinement effect, we have calculated the profiles across the film of two characteristic quantities of the PP segments. One is the profile of the P_2 order parameter for the angle between the PP segments and the normal to the plane of confinement ($\hat{z} = (0, 0, 1)$) and the other one is the length of the PP segments. The location within the film was computed using the geometrical center of the PP segments.

Here, is relevant to mention that we just will consider these observables inside of the called “*center of mass zone*” (marked as CM zone in Figure 10)), i.e., the zone within the film reachable by the centers of mass of chains. Due to the nature of the PP segments, they can exist beyond the space reachable by the center of mass of the chains and that is the reason of why $L_{pp}(P_2$ of $PP_z)$ after achieving a maximum(minimum) goes to zero. We note

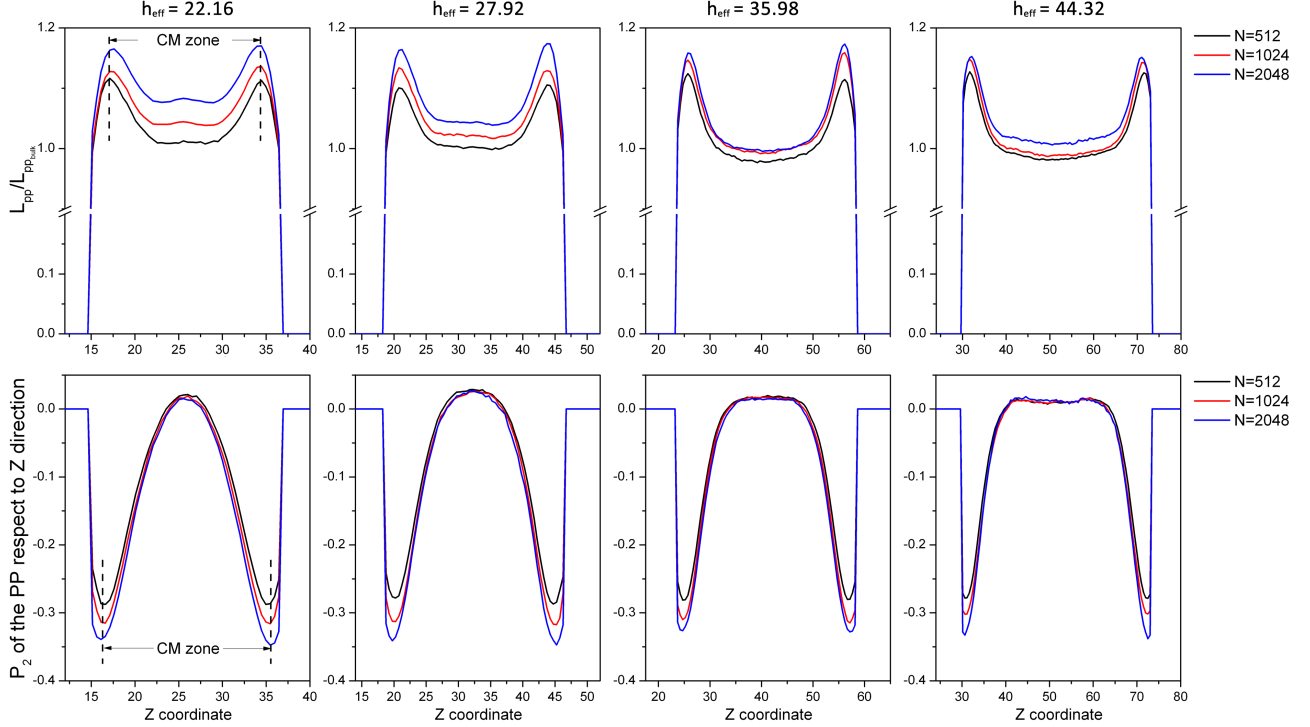


Figure 10: Primitive path characterization. In the top, average PP segment length (L_{pp}) normalized with the bulk value. Bottom, P_2 order parameter evaluated on the angle defined between the PP segments and the $\hat{z} = (0, 0, 1)$ direction. The position in the profile is computed using the geometrical center of the PP segments. The zone delimited by the center of mass of the chains is indicated.

that the location of these extrema coincides with the boundary of the center of the mass zone. Beyond this limit, the data is mostly related to the tails of the chains.

Interestingly, we found that the primitive path segments are quite insensitive to the confinement and the chain-length exhibit two characteristic *weak* response depending on their location within the film. There is a relatively vast region of the center-film where the length of the segments is constant, and at some point, near to the edge, their length increases monotonically, stretching up to 10% – 18%. We note that the starting point for these deviations is at a distance of around one segment length of $L_{pp,bulk}$ from the edge. This seems reasonable if we consider that the segments contributing statistically to this part of the data are in the zone of maximum chain compression and, as we explained before, decreases the number of entanglement locally increasing at the same time PP segments

length. Furthermore, this compression forces the PP to align parallel to the surface of confinement as seen in the bottom graphs showing $P2$ in figure 10, where the negative number indicates perpendicularity with the z -direction.

This behavior seems universal for the PP network and only weakly dependent on the confinement strength and the molecular weight. Only for strong confinement ($h_{eff} = 22.16$, $h_{eff} = 27.92$), the curves obtained for different molecular weights slightly depart from each other by a small vertical shift.

Summary and conclusions

In summary, we have performed an analysis of entanglement statistics in a coarse-grained model of free-standing thin films made out of long linear polymers.

We found that the geometric confinement breaks the isotropic conformation of the chains, compressing and flattening their shape in the direction perpendicular to the plane of confinement as is shown in Figure 9a and 9b. This anisotropic contraction seems not completely compensated in the other direction, and their lateral extension increases by just around 10% ($G_{xx,yy}$ in Figure 9a), which results in an effective decrease of the volume pervaded by the chain.

This decrease in the pervaded volume reduces the number of neighbor chains inside the shared volume, lowering the potential contacts between them, with as chief consequence the effective reduction of entanglements, while the monomer density remains constant. However, the flattening effect is poorly captured by the PP network, as is reported in Figure 10. First, for all chain length under *weak* confinement ($h_{eff} = 44.32$), the PP segments seems to be unaffected and behave in a bulk-like manner for a wide range in the center of the film. It is only near to the surface that the flattening becomes more important, inducing the segments to become parallel to the surface of confinement and increasing slightly (around a 15%) their length. This pronounced change in both observables takes place when the PP is within a

distance comparable to $L_{pp,bulk}$ from the surface.

In the first two graphs of $L_{pp}/L_{pp,bulk}$ in Figure 10 it is notable how, under strong confinement, ($h_{eff} = 22.16 - 27.92$) only the PP segments associated with longer chains shift their length slightly (just around 10% with respect to the bulk value) inside the film while conserving the characteristic effect of increasing near to the film edge.

We also performed a comparison of our data with the theory proposed in Ref. 19, which models the entanglement reduction in confined systems as a function of the strength of confinement. After detailed tests of the central hypothesis, we found evidence that the second hypothesis: “*the oriental correlation at the end-to-end vector scales created by geometric confinement are directly communicated to the primitive path network*”, seems not to be right. In fact, we found substantial evidence that these vectors have uncorrelated orientations, except for a thin layer close to the surface, and this effect is even more notable for longer chains. However, the extension of the Silberberg model proposed by the same authors fits the results for the chain conformation quite well in all the simulated range. A better understanding of the response of the primitive path to global chain deformation would be desirable to generalize the ideas of Ref. 19.

Appendix I

As mentioned in section II, since the interparticle potential used in this study is built with a soft-core repulsion and an attractive tail, depending on the relative weight of both interaction a problem of thermodynamic stability may arise. Thus, to ensure the stability of our system it was necessary to determine a safety range of values for the *independent parameter* w (see Eq. 4).

Originally, the theoretical framework for predicting the stability of these kinds of systems was provided by Fisher and Ruelle.^{26,27} According to Proposition 3.2.2 in Ref. 27 the stability is ensured if the total potential energy U of a given system with N_t particles interacting

through a pair potential $\Phi(r)$ satisfies the inequality:

$$U(\mathbf{r}_1, \mathbf{r}_2, \dots, \mathbf{r}_{N_t}) = \sum_{i=1}^{N_t-1} \sum_{j>i}^{N_t} \Phi(|\mathbf{r}_i - \mathbf{r}_j|) \geq -N_t \varepsilon \quad (7)$$

where \mathbf{r}_i is the vector position of the particle i , and $\varepsilon \geq 0$ is a finite constant independent of N_t . This inequality ensures the convergence of the grand partition function.

Beyond this formal criterion, Fisher and Ruelle also provided two more straightforward rules which help one to decide whether a potential will lead to a steady thermodynamic state. The first criterion is a weaker condition:

$$\int d\mathbf{r} \Phi(r) > 0 \quad (8)$$

which is necessary but not sufficient, i.e., if $\int d\mathbf{r} \Phi(r) < 0$ the system is unstable.

A sufficient condition for stability is that given in Ref. 26

$$\tilde{\Phi}(k) = \frac{1}{(2\pi)^3} \int d\mathbf{r} \Phi(r) e^{-i\mathbf{k}\mathbf{r}} \geq 0 \quad (9)$$

with the following equivalent form:²⁸

$$\tilde{\Phi}(k) = \frac{1}{2\pi^2 k} \int_0^\infty r \Phi(r) \sin(kr) dr \geq 0 \quad (10)$$

that must be verified for all k . Then, applying this criterion to our potential (replacing Eq. 4 in Eq. 10) and integrating, an inequality in terms of w is obtained:

$$\tilde{\Phi}(k) = \frac{\lambda^3 e^{-k^2 \lambda^2} \left(\sqrt{2}(1+w) e^{k^2 \lambda^2 / 2} - 4w \right)}{4\pi^{3/2}} \geq 0 \quad (11)$$

where is easy to see that the sign of this expression is given for the expression inside the

parenthesis:

$$\sqrt{2}(1+w)e^{k^2\lambda^2/2} - 4w \geq 0 \quad (12)$$

as all other terms are positive. Moreover, in Eq. 12 is clear that the term $e^{k^2\lambda^2/2}$ is greater or equal to 1 for all k values, and in particular the inequality is verified independently of w if $k \rightarrow \infty$. Then and since this inequality should be satisfied for all k values, without loss of generality we can take $k = 0$, so the final condition is reduced to:

$$\sqrt{2}(1+w) - 4w \geq 0 \quad (13)$$

which is always satisfied if:

$$w \leq (2^{3/2} - 1)^{-1} \quad (14)$$

Finally, taking w in the interval $0 \leq w \leq (2^{3/2} - 1)^{-1}$ ensures the thermodynamic stability for our system.

Acknowledgement

We are grateful to Prof. Martin Kröger (ETH Zürich) for his help with the $Z1$ algorithm.

References

- (1) Doi, M.; Edwards, S. F. *The theory of polymer dynamics*; Internat. Ser. Mono. Phys.; Oxford Univ. Press: Oxford, 1986.
- (2) de Gennes, P. G. Reptation of a Polymer Chain in the Presence of Fixed Obstacles. *The Journal of Chemical Physics* **1971**, *55*, 572–579.

- (3) de Gennes, P. G. Dynamics of Entangled Polymer Solutions. II. Inclusion of Hydrodynamic Interactions. *Macromolecules* **1976**, *9*, 594–598.
- (4) Edwards, S. F. The statistical mechanics of polymers with excluded volume. *Proceedings of the Physical Society* **1965**, *85*, 613–624.
- (5) Edwards, S. F. The statistical mechanics of polymerized material. *Proceedings of the Physical Society* **1967**, *92*, 9.
- (6) Rayss, J.; PodkořCielny, W. M.; Widomski, J. The properties of polymer protective coatings of optical fibers. I. The influence of active diluent concentration on the properties of UV-cured epoxyacrylate coatings. *Journal of Applied Polymer Science* **1993**, *49*, 835–838.
- (7) Zhang, X.; Bell, J. P. Synthesis of protective coatings on steel by surface spontaneous polymerization. 3: Process development and coating property studies. *Polymer Engineering & Science* **1999**, *39*, 119–127.
- (8) Marencic, A. P.; Register, R. A. Controlling Order in Block Copolymer Thin Films for Nanopatterning Applications. *Annual Review of Chemical and Biomolecular Engineering* **2010**, *1*, 277–297, PMID: 22432582.
- (9) Tsui, O. K. C.; Zhang, H. F. Effects of Chain Ends and Chain Entanglement on the Glass Transition Temperature of Polymer Thin Films. *Macromolecules* **2001**, *34*, 9139–9142.
- (10) Rathfon, J. M.; Cohn, R. W.; Crosby, A. J.; Rothstein, J. P.; Tew, G. N. Confinement Effects on Chain Entanglement in Free-Standing Polystyrene Ultrathin Films. *Macromolecules* **2011**, *44*, 5436–5442.
- (11) Campise, F.; Agudelo, D. C.; Acosta, R. H.; Villar, M. A.; Vallés, E. M.; Monti, G. A.;

- Vega, D. A. Contribution of Entanglements to Polymer Network Elasticity. *Macromolecules* **2017**, *50*, 2964–2972.
- (12) Aoki, H.; Morita, S.; Sekine, R.; Ito, S. Conformation of Single Poly(methyl methacrylate) Chains in an Ultra-Thin Film Studied by Scanning Near-Field Optical Microscopy. *Polymer Journal* **2008**, *40*.
- (13) Chappa, V. C.; Morse, D. C.; Zippelius, A.; Müller, M. Translationally invariant slip-spring model for entangled polymer dynamics. *Physical Review Letters* **2012**, *109*, 1–5.
- (14) Del Biondo, D.; Masnada, E. M.; Merabia, S.; Couty, M.; Barrat, J.-L. Numerical study of a slip-link model for polymer melts and nanocomposites. *Journal of Chemical Physics* **2013**, *138*.
- (15) Masnada, E.; Merabia, S.; Couty, M.; Barrat, J.-L. Entanglement-induced reinforcement in polymer nanocomposites. *Soft Matter* **2013**, *9*, 10532–10544.
- (16) Ramírez-Hernández, A.; Müller, M.; de Pablo, J. J. Theoretically informed entangled polymer simulations: linear and non-linear rheology of melts. *Soft Matter* **2013**, *9*, 2030.
- (17) Ramírez-Hernández, A.; Peters, B. L.; Andreev, M.; Schieber, J. D.; de Pablo, J. J. A multichain polymer slip-spring model with fluctuating number of entanglements for linear and nonlinear rheology. *The Journal of Chemical Physics* **2015**, *143*, 243147.
- (18) Ramírez-Hernández, A.; Peters, B. L.; Schneider, L.; Andreev, M.; Schieber, J. D.; Müller, M.; De Pablo, J. J. A multi-chain polymer slip-spring model with fluctuating number of entanglements: Density fluctuations, confinement, and phase separation. *Journal of Chemical Physics* **2017**, *146*.
- (19) Sussman, D. M.; Tung, W.-S.; Winey, K. I.; Schweizer, K. S.; Riggleman, R. A. Entanglement Reduction and Anisotropic Chain and Primitive Path Conformations in

- Polymer Melts under Thin Film and Cylindrical Confinement. *Macromolecules* **2014**, *47*, 6462–6472.
- (20) Sussman, D. M. Spatial distribution of entanglements in thin free-standing films. *Physical Review E* **2016**, *94*, 1–9.
- (21) Korolkovas, A.; Gutfreund, P.; Barrat, J.-L. Simulation of entangled polymer solutions. *The Journal of Chemical Physics* **2016**, *145*, 124113.
- (22) Korolkovas, A.; Rodriguez-Emmenegger, C.; de los Santos Pereira, A.; Chennevière, A.; Restagno, F.; Wolff, M.; Adlmann, F. A.; Dennison, A. J. C.; Gutfreund, P. Polymer Brush Collapse under Shear Flow. *Macromolecules* **2017**, *50*, 1215–1224.
- (23) Louis, A. A.; Bolhuis, P. G.; Hansen, J. P. Mean-field fluid behavior of the Gaussian core model. *Phys. Rev. E* **2000**, *62*, 7961–7972.
- (24) Brańka, A. C.; Heyes, D. M. Thermodynamic and mechanical stability of many-body systems interacting with coarse-grained bounded potentials. *physica status solidi (b)* **2008**, *245*, 2415–2421.
- (25) Heyes, D. M. Thermodynamic stability of soft-core Lennard-Jones fluids and their mixtures. *The Journal of Chemical Physics* **2010**, *132*, 064504.
- (26) Fisher, M. E.; Ruelle, D. The Stability of Many-Particle Systems. *Journal of Mathematical Physics* **1966**, *7*, 260–270.
- (27) David, R. *Statistical Mechanics: Rigorous Results*; World Scientific Publishing Company, 1999.
- (28) Heyes, D. M.; Rickayzen, G. The stability of many-body systems. *Journal of Physics: Condensed Matter* **2007**, *19*, 416101.
- (29) Subramanian, G. A topology preserving method for generating equilibrated polymer melts in computer simulations. *Journal of Chemical Physics* **2010**, *133*.

- (30) Kröger, M. Shortest multiple disconnected path for the analysis of entanglements in two- and three-dimensional polymeric systems. *Computer Physics Communications* **2005**, *168*, 209–232.
- (31) Shanbhag, S.; Kröger, M. Primitive path networks generated by annealing and geometrical methods: Insights into differences. *Macromolecules* **2007**, *40*, 2897–2903.
- (32) Karayiannis, N. C.; Kröger, M. Combined molecular algorithms for the generation, equilibration and topological analysis of entangled polymers: Methodology and performance. *International Journal of Molecular Sciences* **2009**, *10*, 5054–5089.
- (33) Hoy, R. S.; Foteinopoulou, K.; Kröger, M. Topological analysis of polymeric melts: Chain-length effects and fast-converging estimators for entanglement length. *Physical Review E - Statistical, Nonlinear, and Soft Matter Physics* **2009**, *80*, 14–16.
- (34) Lin, Y. H. Number of entanglement strands per cubed tube diameter, a fundamental aspect of topological universality in polymer viscoelasticity. *Macromolecules* **1987**, *20*, 3080–3083.
- (35) Kavassalis, T. A.; Noolandi, J. A new theory of entanglements and dynamics in dense polymer systems. *Macromolecules* **1988**, *21*, 2869–2879.
- (36) Fetters, L. J.; Lohse, D. J.; Richter, D.; Witten, T. A.; Zirkel, A. Connection between Polymer Molecular Weight, Density, Chain Dimensions, and Melt Viscoelastic Properties. *Macromolecules* **1994**, *27*, 4639–4647.
- (37) Si, L.; Massa, M. V.; Dalnoki-Veress, K.; Brown, H. R.; Jones, R. A. L. Chain Entanglement in Thin Freestanding Polymer Films. *Phys. Rev. Lett.* **2005**, *94*, 127801.
- (38) Liu, Y.; Chen, Y.-C.; Hutchens, S.; Lawrence, J.; Emrick, T.; Crosby, A. J. Directly Measuring the Complete Stress-Strain Response of Ultrathin Polymer Films. *Macromolecules* **2015**, *48*, 6534–6540.

- (39) Cavallo, A.; Müller, M.; Wittmer, J. P.; Johner, A.; Binder, K. Single chain structure in thin polymer films: corrections to Flory's and Silberberg's hypotheses. *Journal of Physics: Condensed Matter* **2005**, *17*, S1697.
- (40) Vladkov, M.; Barrat, J.-L. Local Dynamics and Primitive Path Analysis for a Model Polymer Melt near a Surface. *Macromolecules* **2007**, *40*, 3797–3804.
- (41) Silberberg, A. Distribution of conformations and chain ends near the surface of a melt of linear flexible macromolecules. *Journal of Colloid and Interface Science* **1982**, *90*, 86 – 91.
- (42) Müller, M. Chain conformations and correlations in thin polymer films: A Monte Carlo study. *The Journal of Chemical Physics* **2002**, *116*, 9930–9938.